

# REPORT DOCUMENTATION PAGE

AFRL-SR-AR-TR-03-

Public reporting burden for this collection of information is estimated to average 1 hour per response, including the time for reviewing instructions, data needed, and completing and reviewing this collection of information. Send comments regarding this burden estimate or any other aspect of this burden to Department of Defense, Washington Headquarters Services, Directorate for Information Operations and Reports (0704-01-4302). Respondents should be aware that notwithstanding any other provision of law, no person shall be subject to any penalty for failing to respond to a valid OMB control number. PLEASE DO NOT RETURN YOUR FORM TO THE ABOVE ADDRESS.

0209

1. REPORT DATE (DD-MM-YYYY)	2. REPORT TYPE		
02-10-2003	FINAL REPORT		
4. TITLE AND SUBTITLE			
FLUID-OPTIC INTERACTIONS III (ADAPTIVE-OPTIC)			
6. AUTHOR(S)			
ERIC J. JUMPER			
7. PERFORMING ORGANIZATION NAME(S) AND ADDRESS(ES)			
DEPARTMENT OF AEROSPACE AND MECHANICAL ENGINEERING UNIVERSITY OF NOTRE DAME NOTRE DAME, IN 46556			
8. PERFORMING ORGANIZATION REPORT NUMBER			
9. SPONSORING / MONITORING AGENCY NAME(S) AND ADDRESS(ES)			
AIR FORCE OFFICE OF SCIENTIFIC RESEARCH AFOSR/NA 4015 WILSON BLVD. ROOM 713 ARLINGTON, VA 22203-1977			
10. SPONSOR/MONITOR'S ACRONYM(S)			
11. SPONSOR/MONITOR'S REPORT NUMBER(S)			
12. DISTRIBUTION / AVAILABILITY STATEMENT			
<p style="text-align: center;"><b>DISTRIBUTION STATEMENT A</b></p> <p>Approved for Public Release Distribution Unlimited</p>			
13. SUPPLEMENTARY NOTES			
<p style="text-align: right;">20030326 027</p> <p><b>14. ABSTRACT</b> This report describes fluid-optic interaction research at the University of Notre Dame. When a laser beam propagates through a variable-index-of-refraction, turbulent fluid, its wavefront becomes aberrated, reducing associated optical-system performance. For flight Mach numbers above 0.6 Mach, "compressibility" effects in the flow past the aircraft become important in aberrating wavefronts (aero-optics). This report presents experimental validation for the mechanism responsible for these aberrations in high, subsonic-Mach, free shear-layer flows, the so-called Weakly-Compressible Model. The data collected for this validation clearly shows that deep static pressure wells form in the coherent structures naturally present in shear layers. The presence of these static pressure wells overturns the previously-held belief that static-pressure fluctuations in shear layers are negligible. Results of a study using Proper Orthogonal Decomposition (POD) are also presented. These results suggest that POD methods can be extremely useful in solving some of the high-speed wavefront sensing issues associated with mitigating shear-layer induced aero-optical effects.</p>			
15. SUBJECT TERMS			
Fluid-Optic Interactions, Aero-Optics, Adaptive Optics, Wavefront Sensing, Compressible Shear Layers, Mixing Layers, Turbulence, the Weakly-Compressible Model			
16. SECURITY CLASSIFICATION OF: UNCLASSIFIED		17. LIMITATION OF ABSTRACT	18. NUMBER OF PAGES
a. REPORT UNCLASSIFIED	b. ABSTRACT UNCLASSIFIED	c. THIS PAGE UNCLASSIFIED	UL
			29
			19a. NAME OF RESPONSIBLE PERSON Dr. Thomas J. Beutner
			19b. TELEPHONE NUMBER (include area code) (703) 696-6961

## EXECUTIVE SUMMARY

When a laser beam with an otherwise planar optical wavefront, is made to propagate through a turbulent, variable-index flow field, the beam's wavefront is imprinted with a time-varying aberration over its aperture (beam diameter). These dynamic aberrations degrade the ability for the beam to be focused in the far field. In the case of a laser directed energy weapon on an airborne platform, the far field could be anywhere from kilometers to hundreds of kilometers away. The lethality of an airborne laser weapon depends on the beam-control system being able to hold a spot on the target's aim point, which exceeds a minimum intensity, and hold track so that the product of the beam's intensity and time exceeds a value dictated by the target's hardness. The beam's intensity on target is directly dependent on how well it can be focused. In general, there are two distinct regimes of variant-index flows that contribute to the focusability: the first is the beam's path from just outside the flowfield surrounding the aircraft, through the intervening atmosphere, to the target; and the second is the flow traversed by the beam within the immediate vicinity of the aircraft. The first regime is referred to as "atmospheric propagation." This grant effort specifically addressed the optical-propagation problem in the immediate vicinity of a high-subsonic and transonic airborne platform; this regime of the optical-propagation problem is referred to as "aero-optics." In particular, this effort was concerned with building the knowledge base needed to actively mitigate wavefront aberrations due to laser propagation through *separated shear layers*. AFOSR-funded research at Notre Dame has shown that, although propagation through attached turbulent boundary layers can reduce the intensity on target by 5 – 60%, this reduction in intensity pales in comparison to propagation through a separated shear layer, which can reduce the intensity on target by more than 95%. The problem of understanding how to deal with firing through a separated shear layer has gained new significance in recent years with the DoD's interest, through the Joint Technology Office (JTO), in the design issues related to placing a high-energy laser on a tactical aircraft, ATHEL (Airborne Tactical High Energy Laser). One of the technology areas under the ATHEL initiative is entitled Directed Energy Beam Improvement using Flow eXcitation (DEBI-FX); the principal reference for the DEBI-FX RFP was a paper written under the purview of this grant.

The Notre Dame AFOSR efforts in aero-optics, including the work reported on here, are a success story in research investment, which began less than a decade ago. At that time, aero-optics was considered to be a mature topic, assumed to be treatable only as a stochastic process, and addressable only through statistical methods. This meant that, at best, aero-optics could provide only *the ability to estimate the reduction in lethality that might be incurred due to firing through the flow field next to the aircraft*. Our first effort sought only to answer the questions of what are the temporal and spatial frequencies associated with the beam's aberrations after traversing an aero-optic, aberrating turbulent shear flow. Starting with a concept for extracting statistical data related to answering these questions, we discovered a way to collect correlated time series of the instant-to-instant distorted wavefronts at rates in excess of 100 kHz. Prior to Notre Dame's development of what is now referred to as the Small-Aperture Beam Technique (SABT) wavefront sensor, state-of-the-art wavefront sensors operated at 1 – 2 kHz. Having a truly high-bandwidth wavefront sensor allowed us to begin studying optical propagation through shear layers, starting with the shear layers confining a heated, two-dimensional jet. In cooperation with the Arnold Engineering Development Center (AEDC), we used the SABT sensor to collect the first ever, time-resolved wavefronts for propagation through a Mach 0.8 turbulent boundary layer and separated shear layer that simulated Mach 0.8 flight at 13,500 ft. Comparisons made during this grant period between heated-jet data and the AEDC data revealed a common misconception that, while the spatial and temporal frequencies could be scaled from the heated-jet to compressible shear layers, the mechanism for creating the aberrations was completely different. This led to our development in this grant period of a model for the cause of the aberrations in compressible shear layers, *the Weakly-Compressible Model*. The Weakly-Compressible Model will be described in this report. A large portion of the work under the present grant was devoted to constructing a new shear-layer facility, bringing it on line, and using it to verify the Weakly-Compressible Model. A description of this facility and the validation is contained in this report. The Weakly-Compressible Model allowed the AEDC data to be extended to other flight conditions and aperture sizes. These data, and their extension to other flight conditions, have formed the DoD's basis for systems-design analysis of ATHEL missions and identifying aero-optics as a key technology area. The model was also instrumental in

identifying the aberrating fluid structures in the flow, and this identification was the basis for the DEBI-FX program referred to above.

It has long been known that if a conjugate wavefront is placed on a laser beam prior to its propagation through the aberrating flow, the beam will emerge with a planar wavefront. Systems that sense the aberration, compute the appropriate conjugate wavefont and send commands to a deformable mirror so that the beam may be reflected off of the mirror prior to passing through the aberrating flow are called *adaptive-optic systems*. These systems have been successfully applied to the atmospheric propagation problem to restore focusability to a beam that would otherwise have been degraded. Work performed during this reporting period has shown that the spatial and temporal frequencies required to apply conventional adaptive-optic techniques to mitigating aero-optic aberrations are up to two orders of magnitude greater than those required to correct for the atmospheric propagation problem. If traditional approaches to adaptive optics are taken for the aero-optics problem, adaptive-optic corrections are inconceivable; however, our work has shown that flow control can be used to solve the high-bandwidth problems associated with aero-optics. The basic problem is that too much sensor information needed to acquire wavefronts must be collected and processed to be able to update an adaptive-optic system at the rates required to improve the beams focusability.

In order to speed up this wavefront acquisition, we applied Proper Orthogonal Decomposition (POD) to the aero-optic problem and demonstrated that wavefront measurements can be streamlined using this reduced-order method. Further, we have shown that POD-related methods offer the possibility that wavefront measurements made in a single, fixed direction can be used to predict wavefront distortions in any other direction, providing a near miraculous solution to a major beam-control problem. These POD results will also be described in this report.

## TABLE OF CONTENTS

	Page
EXECUTIVE SUMMARY	i
TABLE OF CONTENTS	iii
TITLE	1
I. INTRODUCTION	1
Defining the Fluid-Optic Interaction Problem	2
Notre Dame's contributions to Advancing the Study of Aero-Optics	3
II. COMPRESSIBLE FREE SHEAR LAYERS	6
First Objective for the Present Reporting Period	8
III. OBJECTIVE 1: VALIDATION OF THE WEAKLY-COMPRESSIBLE MODEL	8
Flow, Coherent-Structure Formation and Static-Pressure Well Results	10
Flow Conditions	10
Flow Visualization of Coherent Structures	11
Static Pressure Data	11
Aero-Optic Data	13
Aero-Optic Comparison with the Weakly-Compressible Model	16
Validation of the Weakly-Compressible Model	17
IV. OBJECTIVE 2: THE APPLICATION OF LOW-ORDER METHODS TO AERO-OPTICS	17
V. CONCLUDING REMARKS	21
Personnel Supported under this Effort	22
Dissemination of Results	22
VI. REFERENCES	23

## Final Report

# Fluid-Optic Interactions III (Adaptive-Optic)

AFOSR Grant F49620-00-0025

Principal Investigator: Eric J. Jumper  
Hessert Laboratory  
Department of Aerospace and Mechanical Engineering  
Center for Flow Physics and Control  
University of Notre Dame  
Notre Dame, Indiana, 46556, USA  
(574) 631-7680  
FAX: (574) 631-8355  
Email: jumper.1@nd.edu

## I. INTRODUCTION

It is difficult to write a final report on a program that is completing its third round of funding, each with a significant number of breakthroughs, and a program that will be continuing beyond this reporting period. The difficulty lies in the fact that the objectives and accomplishments of this reporting period can only be understood in the context of the accomplishments of the previous grants. Although these earlier accomplishments have already been reported in two previous *Final Reports* (*F49620-93-0163* and *F4920-97-1-0489*), I feel that a relatively complete reporting of the overall accomplishments of the research belongs in this document in order to properly report the accomplishments of the present reporting period. As such, this *Introduction* contains a definition of the fluid-optic interaction problem, a brief commentary about Notre Dame's development of Small-Aperture Beam Technique wavefront sensor (SABT sensor) and the SABT's impact on the study of fluid-optics. This is followed by some of the things we have learned using the SABT about the nature of the aberrating effects imposed on a laser due to propagation through free shear layers, as well as the adaptive-optic requirements for mitigating them. Because of the significance of our discovery of the aberration physics associated with a compressible, free shear layer, rather than including a discussion of this physics in the *Introduction*, a complete section is devoted to optical propagation through weakly-compressible, free shear layers, culminating in a description of the *Weakly-Compressible Model*. That section ends with a statement of the first of two objectives of the present reporting period, that being an experimental validation of the Weakly-Compressible Model; *Section III* of this report will describe the results of that validation. The final section of this report will describe the progress that we have made on the second objective of this reporting period, which was to investigate the applicability of lower-order methods to the problem of measuring wavefront aberrations imposed on a laser due to optical propagation through free shear layers. The results of our initial study into this question are probably the most important discoveries of this reporting period, and, as will be described in *Section IV*, show the first evidence of the possibility of using a

beacon in some fixed direction to be able to predict the wavefront aberrations due to propagation in other directions.

### ***Defining the Fluid-Optic Interaction Problem.***

The transmission of a collimated light beam, of “viewing aperture”  $A$ , through a turbulent flowfield with index-of-refraction variations, leads to a time-varying aberration of its otherwise-planar, optical wavefront. These aberrations lead to a reduction in performance of an optical system making use of the optical “information” contained over the viewing aperture. Systems concerned with such reduction in performance include, but are not limited to, airborne imaging systems and airborne laser irradiating systems. These latter systems include airborne laser weapons such as the Air Force’s Airborne Laser (ABL) theater ballistic defense system, Extended Range (ER) versions of ABL, Tactical Aircraft High Energy Laser systems (TAHEL), and airborne free-space communication systems. These effects also impact ground-based astronomical systems such as those used for imaging satellites. In this case, both atmospheric turbulence and wind-induced shear and boundary layers over the viewing aperture degrade the system performance. Thus, it is clear that Fluid-Optic Interaction problems directly impact both the Air Force’s atmospheric and space missions.

A system’s performance reduction (induced by turbulent, variant-index flowfields) can be quantified by analysis of the far-field irradiance pattern [Ref.1]. The irradiance pattern is the instantaneous intensity pattern at the target,  $I(x,y,t)$ , where  $(0,0)$  would indicate the center of the aim point. The extent to which the on-axis intensity is reduced as a function of time,  $I(0,0,t)$ , when divided by the highest possible on-axis intensity without aberrations (referred to as the diffraction-limited intensity),  $I_o$ , is expressed as the Strehl ratio,  $S_t$ ,

$$S_t(t) = \frac{I(0,0,t)}{I_o}$$

The reduction in Strehl ratio due to time-varying, aberrating fields can occur over short path lengths in the *near field* (i.e., path length,  $z$ , on the order of  $A$ ), or can occur over extended paths (i.e., path lengths,  $z$ , much larger than  $A$ ). The former, short-path (near-field) aberration is usually termed *aero-optics* and the latter, long-path aberrations are usually termed *atmospheric propagation*. These classifications have their origin in the specific applications with which they are associated [see Refs. 2 and 3, for example]. It has long been known that placing a conjugate waveform on the beam prior to its transmission through the aberrating medium results in the emergence of a planar-wavefront beam as it leaves the medium; systems that sense the aberration, construct and apply the proper conjugate waveform at regular time intervals are termed *adaptive-optic systems*, and the study of such systems is known as *adaptive optics* [Ref. 4]. The determination of the design requirements for such systems depend on understanding the spatial and temporal frequencies of the distorted optical wavefront for the applicable aberrating flowfield.

Over the last decade and a half, progress has been made in both measuring the wavefront dynamics for the atmospheric propagation problem and using this information for designing and applying adaptive-optic equipment and techniques [Ref. 5]. For aero-optic problems, on the other hand, while progress in thinking about adaptive-optic correction has been made in the last half decade, *no adaptive optic correction for the aero-optic problem has yet been demonstrated*. The reason for this is that the required spatial and temporal frequencies associated with aero-optic problems are at least an order of magnitude greater than those presently correctable by adaptive-optic systems for the atmospheric-propagation case, even for relatively-slow laboratory flows [Refs. 6]. As such, the main research thrust in aero-optics until the early to mid 1990’s had been to attempt to quantify the time-averaged phase variance (or root-mean-square Optical Path Difference,  $OPD_{rms}$ , which is related to the

phase variance through the wave number). Once obtained by whatever means, the phase variance was used to compute *an estimate* of the system degradation imposed by the near-field aberrations using the large-aperture approximation [Ref. 7]. But, notice that these statistical methods gave no information useful to the design of adaptive-optic systems required to correct aero-optic aberrations. Research at Notre Dame supported by AFOSR has focused exclusively on the *aero-optics problem*, with an emphasis on understanding how *adaptive optics* can be applied to the problem

### ***Notre Dame's Contributions to Advancing the Study of Aero-Optics.***

To understand how far Notre Dame's aero-optic research has progressed since our first grant, it is helpful to divide the understanding of the general fluid-optic interaction problem into four levels, which may be applied to either atmospheric propagation or the aero-optics. These levels can be arranged in their order of complexity as follows: first, there is the level of understanding that allows one to estimate the statistical level of optical distortion that is likely to be encountered for a particular optical propagation scenario through a flowfield/atmosphere. The second level is to be able to predict, not only the statistically-averaged distortion, but the spatial and temporal frequencies associated with the time-varying optical distortion. The third level is to be able to measure actual time histories associated with the optical distortions and link such histories to the specific fluid-mechanic character of the flowfield/atmosphere. The fourth level is to be able to measure the optical distortions rapidly enough to be able to somehow compensate for the distortions so as to improve/restore the optimal performance of the optical system through the use of adaptive optics.

The atmospheric propagation problem has advanced through all four levels of understanding; on the other hand, until Notre Dame's entry into this area of study, aero-optics remained at level one, and researchers in the field had no prospects or apparent aspirations to move to a higher-level of understanding [Refs. 8,9]. Reference 9 was published in 1992 and reported on the most up-to-date methods being applied to aero-optics as of that date. Our first grant began one year later in 1993, and the goals of that effort were only to advance the understanding of aero-optics to include statistical estimates of the spatial and temporal frequencies involved, i.e., to move the understanding to level two. As it happened, we realized that it was possible to build a wavefront sensor rapid enough to capture the time history of an aero-optically distorting wavefront, the SABT sensor [Ref. 10].

The aero-optic problem has always been inextricably linked with the fluid mechanics of turbulent flows. This is in contrast to the atmospheric-propagation problem, which has been treated almost exclusively as an optical problem. For astronomical observations, assuming that viewing conditions are favorable, the aberrating structures are large compared to the viewing aperture. Often these structures are of such extent that the aberrations can be treated as simple tip-tilt corrections [Ref. 5] and smaller aberrations are still relatively large with respect to the aperture, so that only the first few aberration modes need be addressed in order to restore much of the aberration-degraded system performance. These facts mean that the spatial resolution of a wavefront sensor to detect the aberrations in an atmospheric-propagation application need not be exceptionally high. Beyond this, the aberrations move through the viewing aperture at speeds associated with atmospheric winds plus any slue rates that may be superimposed. Typical rates required to provide time-resolved measurements of the aberrated wavefronts due to propagation through the atmosphere are on the order of hundreds of Hertz. Wavefront sensor technology has long been capable of achieving these rates [Refs. 4,5], which explains why progress through all four levels of understanding has been possible for atmospheric propagation.

The aero-optic problem, by its very nature, must contend with shear-layer and boundary-layer aberrations whose sizes are on the order of the associated turbulent structures; further, the convection

rates are now associated with the defining flows which can be much higher than typical atmospheric winds (in the case of flow over an aircraft in flight, for example). Our efforts have shown that even for a laboratory flow of less than 10 m/s, because of the small size of the turbulent structures, wavefront capture rates of 5 kHz are needed to time-resolve the dynamics of the aero-optic wavefront aberrations.

Prior to Notre Dame's invention of the Small-Aperture Beam Technique (SABT) wavefront sensor, the fastest wavefront sensors available operated at less than 1 kHz. At the time of its invention, we were looking into estimating the spatial and temporal frequencies associated with propagation through an aero-optic flow field, that is to say to attempt to move the understanding to level two. Work performed in the late 1980's, had suggested to us that there might be a way of measuring these spatial and temporal frequencies. References 11 and 12 describe a simple optical device, that when coupled with certain fluid-mechanic principles, was capable of directly measuring the statistical  $OPD_{rms}$ , and we felt that the device could be used to extract the frequency data as well. We soon came to realize that the fundamental assertion upon which the instrument of References 11 and 12 was based had the potential of being used to develop an actual wavefront sensor. Indeed, it was possible and led to Notre Dame's development of the SABT (Small-Aperture-Beam Technique) wavefront sensor [Ref. 7,10,13]. The SABT sensor made possible, for the first time, the ability to examine the time-resolved dynamics of the aero-optically aberrated wavefront.

Following the common presumption at the time, we assumed that studying aberrations associated with optical propagation through turbulent shear flows made up of fluids of dissimilar index of refraction would teach us about aberrations due to propagation through compressible shear flows around high-Mach aircraft; to some extent this was true, however, as will be discussed in the next Section, the actual mechanisms causing the aberrations are completely different. We began by extensively studying the aberration characteristics for propagation through the transitional region of a heated, two-dimensional jet. Figure 1, produced using a numerically-simulated flowfield, is helpful in understanding the nature of the optical aberrations produced by propagation through the shear layers comprising the two-dimensional heated jet [Ref. 14]. At an instant in time, an initially-planar wavefront propagates through the aberrating flowfield, also shown at that instant, and emerges with the distorted wavefront shown. In this case, the aberration is due to the mixing of dissimilar index-of-refraction flows. Although the distortion is due to a path integration through the flow, it is possible to associate features on the wavefront with flow features. As the flowfield convects and evolves, a footprint of the character of the evolving flowfield is captured by the wavefront; a time series of the instantaneous wavefronts cut in the streamwise direction, as shown at the upper portion of Fig. 1, captures the dynamics of the shear layers of the two-dimensional jet. The characteristic hills and valleys, and slopes of the features with time, indicate the convective and evolving nature of the flowfield; different structures convect at different rates as evidenced by the different slopes of the hills and valleys. The fact that the shear-layer roll up is organized can be seen by the well-ordered nature of the time series of wavefronts. An actual time series of experimentally-measured wavefronts from the heated-jet experiments is shown in Fig. 2; it is clear that the features found in the simulated field are present in the experiments.

From time series of the Fig. 2 type, time series of far-field irradiance patterns (i.e., intensity distributions at the target plane) can be computed using Fourier Optics [Ref. 15]. The top portion of Fig. 3 (small figures 1 and 2 in Fig. 3) shows one such realization and its concomitant far-field irradiance pattern. If at this same instant in time, the beam were first made to reflect off a mirror deformed into the conjugate of the wavefront error that a planar wavefront would have acquired by propagating through the turbulent fluid, then the beam would emerge as a planar wave. In such a case the far-field irradiance pattern would be a diffraction-limited spot, as shown in the middle of Fig. 3 (i.e., small

figures 3 and 4) for a square aperture. A streamwise cut of this irradiance pattern is plotted as the closest wavefront in the lower portion of Fig. 3 (small figure 6). If this deformable mirror (DM) correction is left on the mirror for some period of time before a new correction is imposed, the on-axis

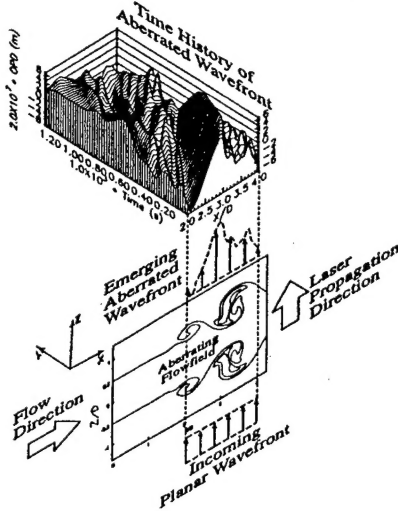


Figure 1. Schematic of a planar wavefront propagating through a two-dimensional heated jet and concomitant time series of one-dimensional, aberrated wavefronts. [Ref. 14]

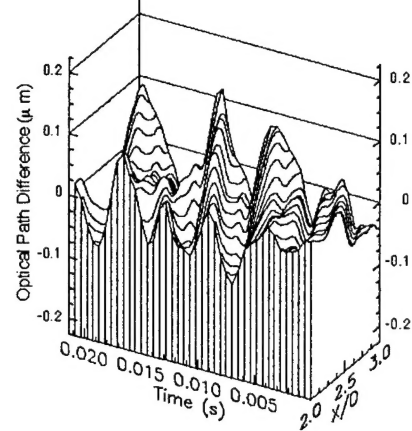


Figure 2. Space-time representation of SABT-measured OPDs for propagation through an experimental, two-dimensional, heated jet flowfield [Ref. 7]

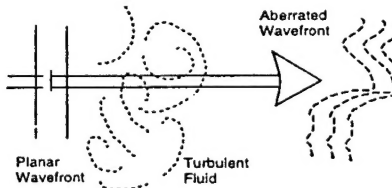


Figure 1: Phase Error Imposed on Wavefront by Fluid

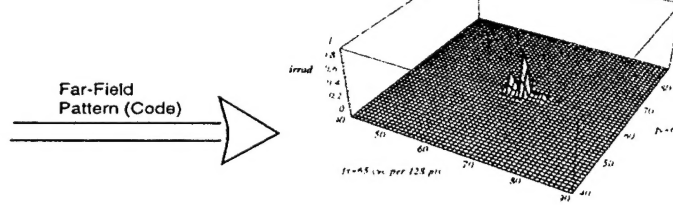


Figure 2: Far-Field, Irradiance Pattern Due to Phase Error

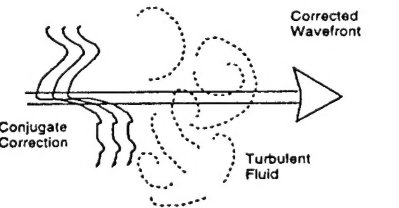


Figure 3: Adaptive-Optically-Corrected Wavefront

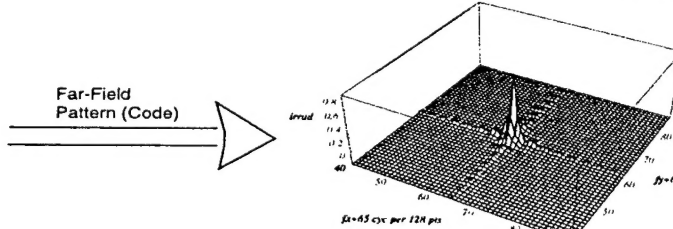


Figure 4: Impulse Response for a Square Aperture

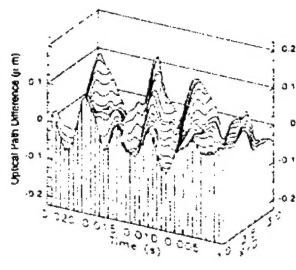


Figure 5: Space-Time Representation of Reconstructed OPD's

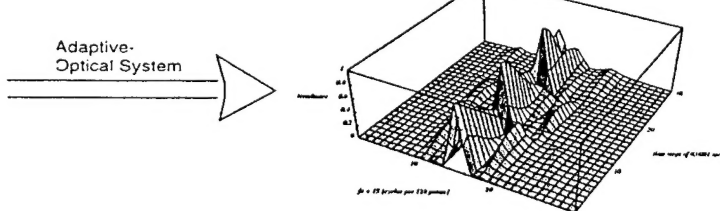


Figure 6: Time Evolution of Far-Field Irradiance

Figure 3. Effect of distorted wavefront on the far-field irradiance pattern (1,2), Effect of a perfect-conjugate correction to produce a diffraction-limited far-field irradiance pattern (3,4), and cuts through the far-field irradiance pattern as a function of time, with periodic, perfect-conjugate corrections imposed on the heated-jet aberrations (5,6) [Ref. 14].

intensity would decay as energy spreads into the wings; then, when a perfect-conjugate correction is again imposed, the on-axis intensity would peak up again and decay until another correction is imposed, etc [Ref. 14]. Although long since established with absolute certainty, the validity of using Fourier Optics to compute the far-field irradiance pattern was beautifully demonstrated by Yanta et. al., who simultaneously measured both the near-field wavefront and the far-field pattern and compared the Fourier-Optics-computed pattern with the measured pattern; they were virtually identical [Ref. 16].

## II. COMPRESSIBLE FREE SHEAR LAYERS

During a previous reporting period, Notre Dame used the SABT sensor to measure the wavefront dynamics for propagation through the Mach 0.8 compressible shear layer at the Arnold Engineering Development Center (AEDC) [Ref.17]. Figure 4 shows two example time series of experimental wavefronts from those tests (5 cm aperture); these data were taken at two stations, Station 1, right at the splitter plate, and Station 2, half a meter downstream from the splitter plate.

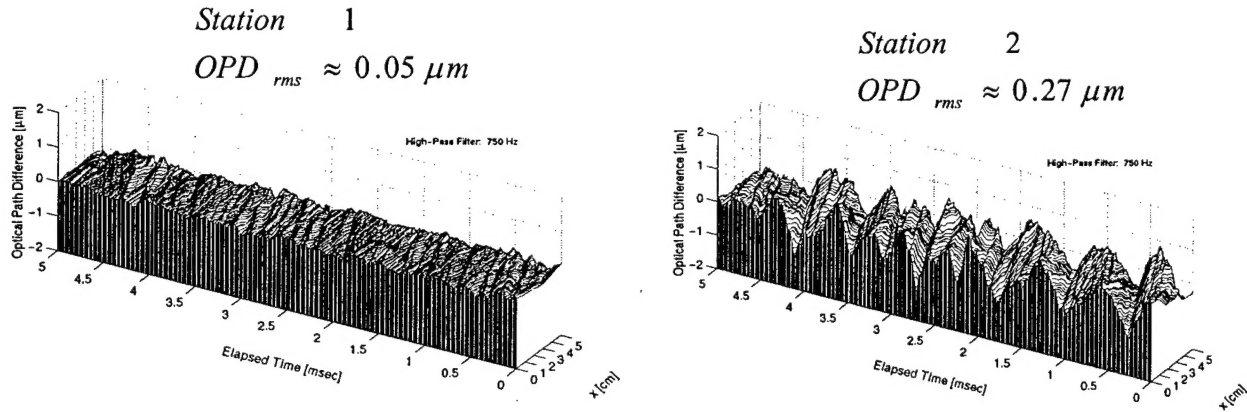


Figure 4. Wavefront Measurements Taken for Propagation through the AEDC Compressible Shear Layer Facility at a Simulated Flight Mach Number of 0.8 at 13,500 ft [Refs. 17,21].

Prior to the work that will be reported for this reporting period, these AEDC data were the only wavefront data of that kind. What is most noteworthy in the data shown in Fig. 4 is the difference in aberration extent between the Station 1 and Station 2 data. The Station 1 data is due to the turbulent boundary layer feeding the shear layer and/or over the extraction window. Even without boundary layer treatment to remove these aberrations, the level of aberration is quite low. For a one-micron-wavelength beam the reduction in Strehl ratio can be estimated to be 0.906 using the large-aperture approximation. It might be noted that the Station 2 data contains cyclic tilt, but even when this is removed, computed far-field patterns yielded a time-averaged Strehl ratio of 0.07 [Ref. 18].

The AEDC wavefront data and their implications on system performance as inferred from computations of the Strehl ratio were clearly of interest to programs such as a TAHEL weapon system; however, they would be more helpful if they could be scaled from the single experimental condition (altitude, Mach number and aperture size) to other relevant conditions. Realistic beam diameters for a HEL weapons system will not be smaller than 20 cm, for example, and any systems studies would require estimates of beam quality for an entire range of Mach numbers and altitudes. This led us to our most-important discovery during the previous reporting period. Our earliest attempts to predict the aberrating effect of the AEDC experimental conditions using the aberration physics, thought at the time to explain the phenomena, failed miserably in predicting the data; this led us to take a new look

at what might be causing the aberrating quality of the flow. The result of this new look resulted in our development of the *Weakly-Compressible Model*.

The key realization at the heart of the Weakly-Compressible Model is the fact that because of the Kelvin Helmholtz instability, free shear layers naturally form coherent structures and, in a frame convecting with the layer, the flow in the coherent structures has high curvature (see Fig. 5) [Refs. 19,20]. This curvature has a concomitant pressure gradient that lowers the pressure at the center of the structures (by several psi in the case of near-transonic shear layers). The low pressure is accompanied by a reduction in the density, which in turn lowers the index of refraction. It is this variation in the index of refraction that causes nearly all of the aero-optic aberrations in weakly-compressible shear layers. As discussed in References 19 and 20, all other aberrating influences present in a shear layer, fed by a common total temperature, have effects that add up to only a small fraction ( $\sim$  order of magnitude less) of this principal cause. Although, this cause-and-effect explanation appears to be straight forward, it had long been thought (i.e., common knowledge) that static-pressure variations in a free shear layer were negligible, the so-called strong Reynolds analogy; the Weakly-Compressible Model argues exactly the opposite.

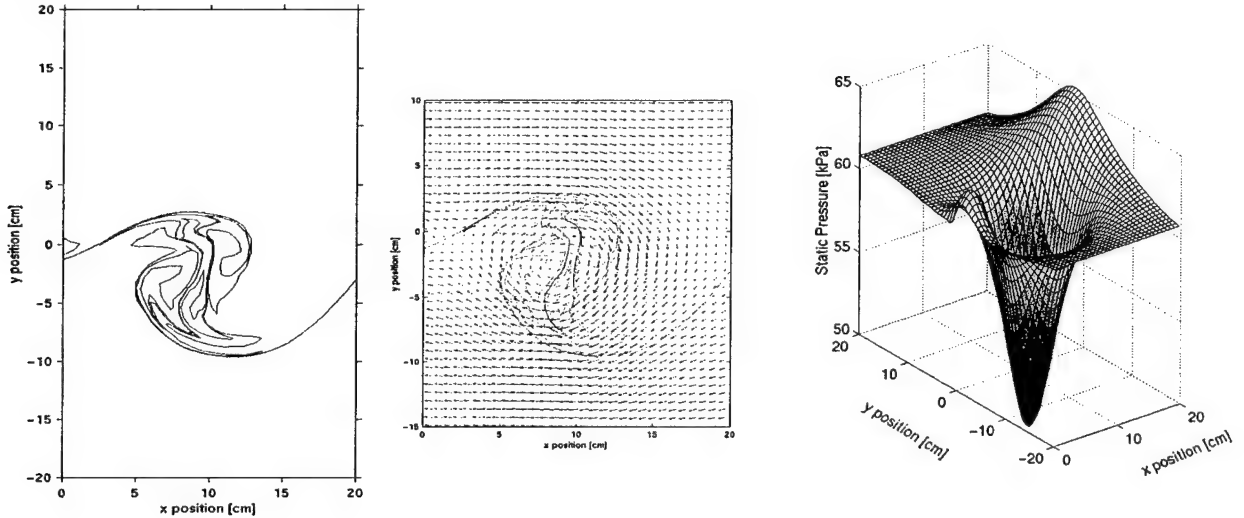


Figure 5. Coherent structure at an Instant in Time, its Flow field as seen in the Convective Frame and its Concomitant Pressure Well as Computed by the Weakly-Compressible Model [Refs. 19,20].

When the model was used to compute the AEDC conditions, it showed excellent agreement in the large-scale structures, but did not predict the higher-frequency aberrations in the data. Further analysis convinced us that the higher-frequency aberrations were due to the turbulent boundary layer over the extraction window of the tunnel. To simulate the addition of the boundary layer aberrations, an aberration time series from AEDC Station 1 (as on the left of Fig. 4, which is due to a turbulent boundary layer) was added to the Weakly-Compressible Model predictions. The comparisons are shown in Fig. 6, which shows the simulation for the AEDC Station 2 conditions in the upper left hand, the AEDC Station 2 data in the lower right hand, and the result of adding the Station 1 wavefronts (upper right hand) to the simulations, resulting in the lower left hand time series. It is clear that the two bottom time series, the simulation and the data, compare well [Refs. 19, 20]. Having the model enabled us to infer that the tilt in the Station 2 data was really a ramification of a larger coherent structure convecting past the 5 cm aperture used in the AEDC experiments. Using our model, we were also able to show that over the larger aperture the  $OPD_{rms}$

increases to 0.451 microns, none of which can be removed by tilt corrections. In this case the Strehl ratio dropped to 0.011 [Ref. 21]. Finally, with the help of the model, we were able to scale the aberration effects measured at the AEDC conditions over the small 5 cm aperture, not only to larger apertures, but also to other altitudes and Mach numbers [Ref. 22].

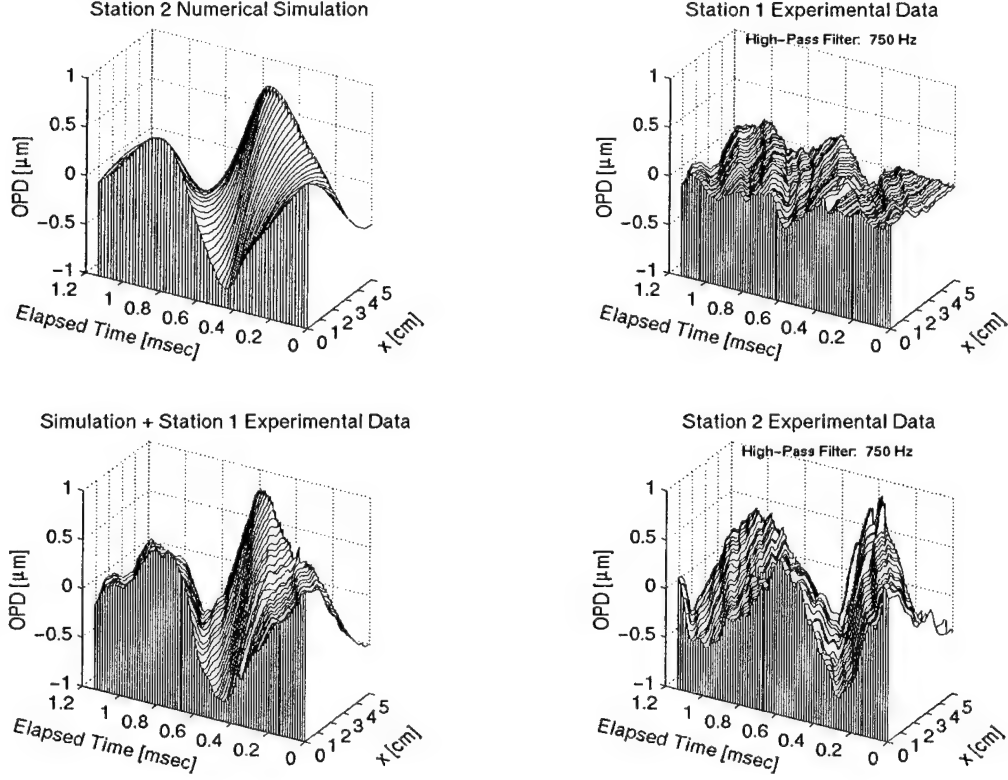


Figure 5. Example Time Series of Wavefronts: the Weakly-Compressible-Model-computed wavefronts for the AEDC, Station 2 conditions (upper left); compared to the Station 2 experimental wavefronts (lower right); when the Station 1 wavefronts (upper right) are added to the computed wavefronts, the comparison is even better (lower left) [Refs. 19,20].

### ***First Objective for the Present Reporting Period***

All of the work reported to this point was the result of accomplishments during previous reporting periods. To that point, the Weakly-Compressible Model's validity rested solely on good agreement with the AEDC *wavefront* data, as in Fig. 5. Because of the importance of, not only the AEDC data, but the extension of that data to other aperture, Mach number and altitude scenarios, made possible by the model, it was important that the model be validated in more than just its integrated effect. *In this regard, the first objective of the research for this reporting period was to independently validate the Weakly-Compressible Model.* In order to do this a new Weakly-Compressible Shear Layer Facility was to be built at Notre Dame for the purpose. In addition to making new aero-optical measurements in the new facility, the most controversial component of the model was to be experimentally investigated, the large pressure wells postulated to be present in the coherent shear-layer structures.

### **III. OBJECTIVE 1: VALIDATION OF THE WEAKLY COMPRESSIBLE MODEL**

As noted in the last section, the first task in validating the Weakly-Compressible Model was to build a new free-shear-layer facility. To this end, a high-Mach, free-shear-layer facility with similar dimensions to the AEDC facility was designed and constructed at Notre Dame in the Hessert Laboratory. The major dimensional dissimilarity to the AEDC facility was in the cross-flow, or spanwise direction; the Notre Dame facility is only 3.81 cm in the span direction, while the span for the AEDC facility was approximately 30 cm. The new shear-layer facility consists of the addition of a new inlet nozzle and test section to one of Notre Dame's three existing transonic in-draft wind tunnels. The fixed portions of these tunnels consist of three differing-dimension diffuser sections that are attached to a large, gated plenum. The plenum is connected to three Allis Chalmer 3,310 CFM vacuum pumps. Depending on the gate-valve arrangements, each of these pumps can be used to power separate diffusers, or they can be used in combination to power a single diffuser. In the present case, only one pump was used to power the free-shear-layer facility. The general arrangement of the facility is shown in Fig. 6.

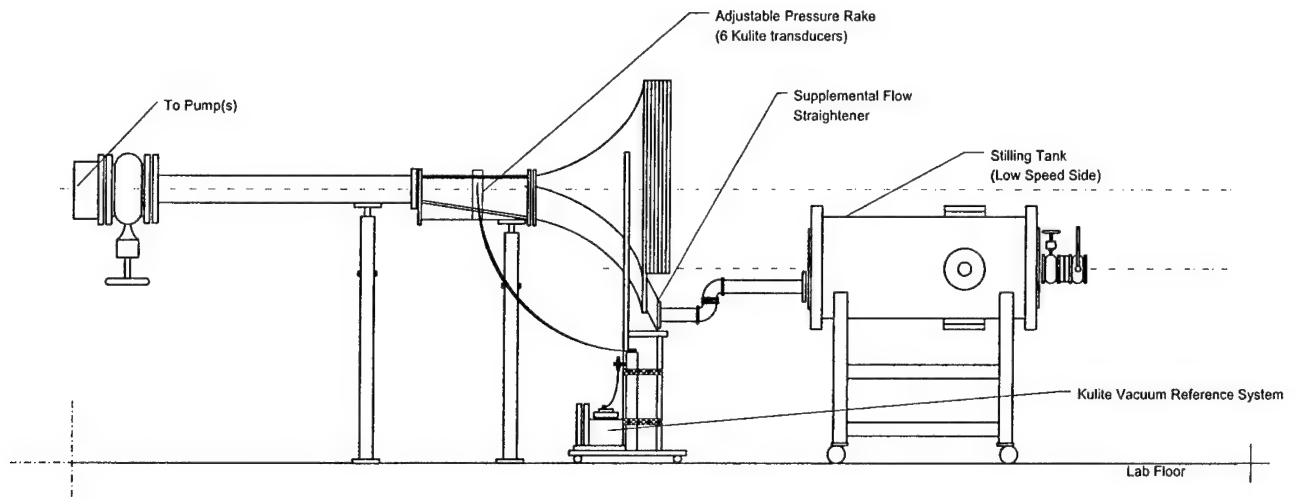


Figure 6. Schematic of the Notre Dame High-Mach Free-Shear-Layer Facility.

Being an in-draft tunnel, the feeding source is the room total pressure and temperature. The test section is fed from a 104-to-1 inlet nozzle directly from room total pressure on the high-speed side. On the low-speed side, room-total-pressure air is first passed through two gate valves to lower its total pressure, while keeping its total temperature the same as the high-speed side's. The air then enters a large stilling tank, where it is used to feed a slightly-diffused flow duct which contains one stage of flow straighteners before feeding the low-speed side of the shear-layer test section. By adjusting the vacuum-pump plenum and diffuser pressure, and by adjusting the stilling chamber total pressure, a range of shear layer conditions can be achieved. The highest Mach number achievable on the high-speed side is Mach 1.09, which is the condition to be presented in this report.

Figure 7 shows a close-up schematic of the test section. Notice that the test section was instrumented with six surface-mounted, 5 psid, Kulite ultra-miniature pressure transducers in the section side wall, aligned in the vertical ( $y$ ) direction at a streamwise ( $x$ ) location of 0.5 m from the splitter plate. These transducers were spaced 1.9 cm apart and could be adjusted as a block in the vertical direction. In addition, there were time-averaged, static pressure ports aligned in the  $x$  direction at intervals of 3.8 cm. The test section had facility for placing a height-adjustable ( $y$ ) pitot pressure probe 1 mm downstream ( $x$ ) from the splitter, in order to document the velocity and

Mach number of the inlet streams feeding the shear layer. The sidewalls of the test section were made of  $\frac{3}{4}$  inch Plexiglass with sufficient optical quality to take Schlieren images of the flow. The upper and lower section walls can be fitted with optical flats for eventual aero-optic studies. These aero-optic windows will allow for a 3.5 cm by 25.4 cm aperture, thereby relieving the aperture limitations of the AEDC studies referred to earlier.

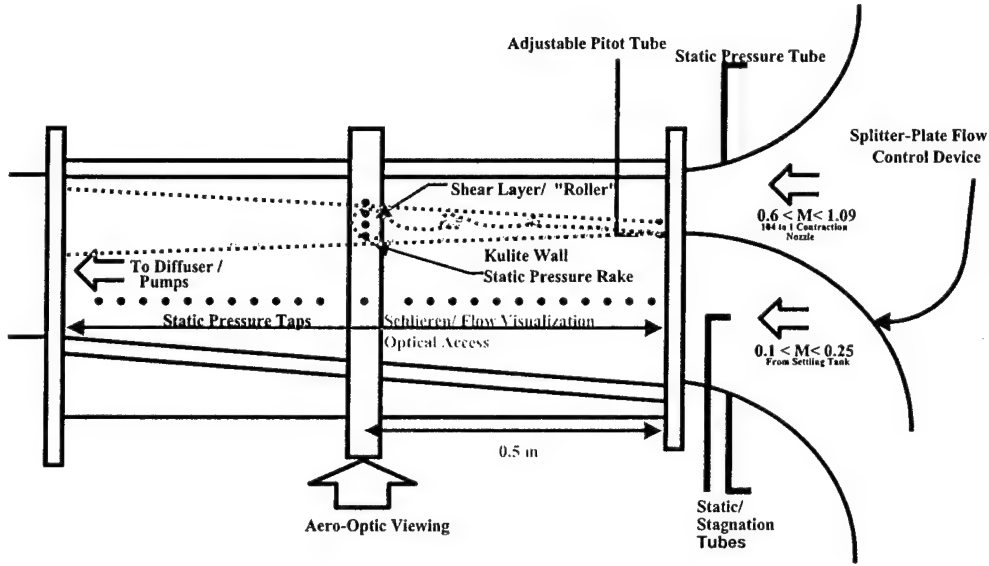


Figure 7. Close-up Schematic of the Test Section.

### **Flow, Coherent-Structure Formation and Static-Pressure Well Results**

As reported in Reference 23, the shear layer was set to run at the highest high-speed-side Mach number achievable, Mach 1.09. The static pressure and temperature in the high-speed side corresponded to a pressure altitude of 21,300 ft. (6.5 km) on +5°C hotter-than-standard day. The low-speed side for these experiments was set to a Mach number of 0.17.

**Flow Conditions.** The flow Mach numbers (1.09 and 0.17) on the high- and low-speed sides of the splitter plate corresponded to Reynolds numbers of  $13.5 \times 10^6 \text{ m}^{-1}$  and  $2.34 \times 10^6 \text{ m}^{-1}$ , respectively. The convective Mach number for this case was 0.43, which was computed by dividing the convective velocity by the speed of sound for the high-speed side of the shear layer [Ref. 23]. Figures 8 and 9 show the flow velocities and Mach numbers at this location as measured by the pitot probe. It can be noted that there is a small deficit in the velocity field 1 mm downstream from the splitter plate, consistent with the boundary layers feeding the shear layer. The high-speed side boundary layer is relatively thin at 2.5 mm. While the low-speed side's boundary layer is approximately 3.4 mm.

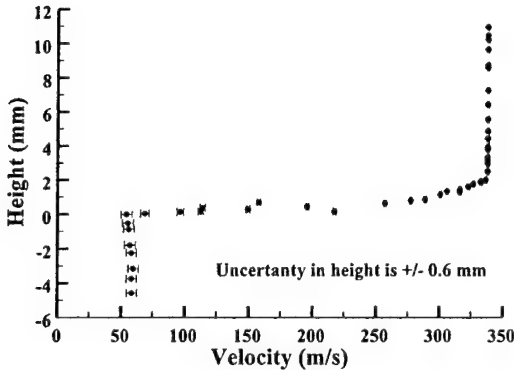


Figure 8. Velocity Field at the Splitter Plate.

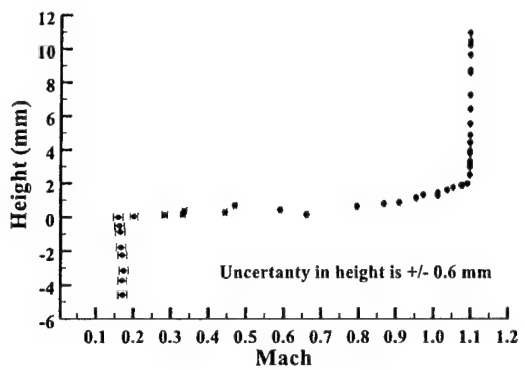


Figure 9. Mach Number Field at the Splitter Plate.

**Flow Visualization of Coherent Structures.** In keeping with the objective of determining the validity of the Weakly-Compressible Model, the first task was to assure that the shear layer was rolling up into coherent, Kelvin-Helmholtz-induced, spanwise structures. Serendipitously, the humidity in the South Bend area is often sufficient so that the static temperature of the flow captured in the coherent structures of the shear layer falls below the dew point, resulting in water vapor



Figure 10. Three Flow Vapor Visualizations of the Coherent Structures in the Shear Layer.

formation. A strobe was used to provide frozen realizations of these structures. Although the shear layer was not forced, which would serve to regularize the formation of the vortical structures, the Kelvin-Helmholtz instability led to repeated rollups that were roughly, although not perfectly, periodic. When the strobe was flashed at the structure passage frequency (or subharmonics of that frequency) a coherent structure could be seen at the 0.5 m and greater  $x$ -locations. Figure 10 shows three realizations of different coherent structures, each at a slightly different stage of development. It should be noted that the vapor only forms in the low-pressure wells of coherent structures; thus the fact that the not-fully formed structure appears, means that the vapor has formed in previous smaller structures, which must pair and pair again, etc. until the larger structures develop. Evidence of the previous structures can be seen as small pinwheel structures along the left braids in the images. The strobe frequency used to capture these realizations had a fundamental of approximately 1.1 kHz. The structures visualized in Fig. 10 may be compared to the computed structures in Fig. 5; it is clear that coherent structures postulated by the Weakly-Compressible Model are indeed present in the shear layer.

**Static Pressure Data.** As the coherent structures passed by the 0.5 m  $x$ -location, the array of sidewall-mounted Kulites measured the static pressure. Keeping in mind that any particular coherent

structure will be at a slightly different stage of formation from any other and will have a slightly different trajectory from any other structure, a continuous time series of static pressures at a fixed  $y$  location is, in general, unlikely to capture a time-position cut through the same location of a repeated coherent structure. Thus, a method was devised to trigger the data acquisition in such a way as to repeatedly capture essentially the same time-position cut through similar structures.

The method devised was to use the Kulite closest to the centerline of the shear layer to trigger the data acquisition when a low-pressure threshold was reached. This threshold was set low enough that the trigger fired only when the pressure reached an absolute minimum. Once triggered, 2048 measurements were collected at each transducer location at 50 kHz. Two hundred such sets of data were collected at each transducer location and then ensemble averaged.

Figure 11 is an example of an ensemble average of 200 phase-locked data series overlaid with a single data series, displaced upward by 2 kPa. It can be seen that after the first cycle, the averaging reduces the amplitude of oscillation of the static pressure; whereas, the single trace continues to have large excursions in amplitude compared to the ensemble averaged trace. What does seem to be captured is the essential character of the static pressure fluctuation over the first cycle, which is the cycle that triggered that data trace. The passage frequency can also be extracted from the ensemble average and can be seen to be approximately 1.1 kHz, consistent with the frequency used to visualize the coherent structures, which was referred to earlier. Notice that the cycle at approximately 0.01 seconds is quite similar to the first cycle in the single trace.

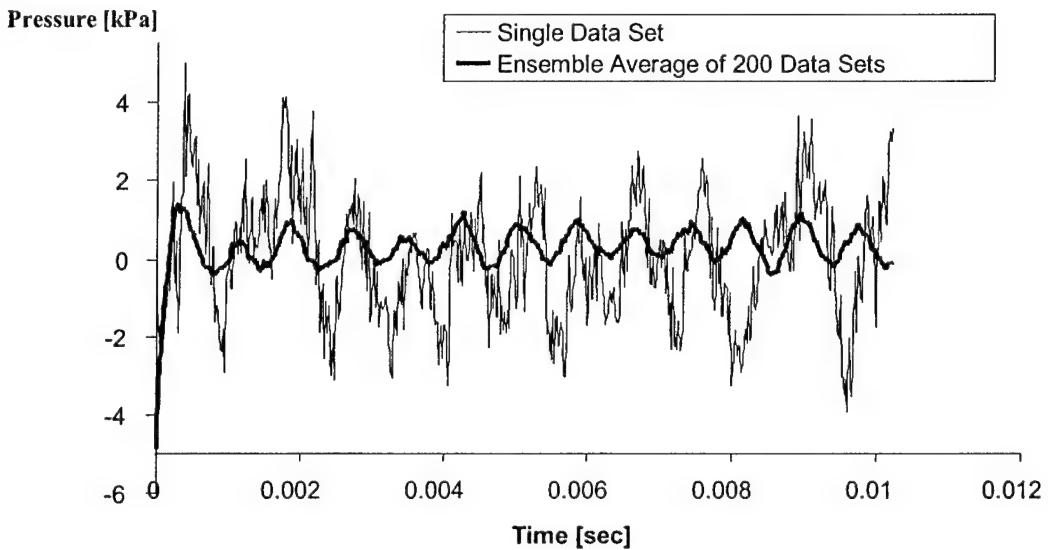


Figure 11. Phase-Locked Average of 200 Trigger Traces Overlaid by a Single Trace.

Figure 12 gives the measurement-location-averaged trace of the 200-ensembled, phase-locked-averaged traces for the first cycle of all six transducer positions overlaid. By measurement-location-averaged we mean that the transducer closest to the centerline of the shear layer was used for the trigger and the other transducers captured the concomitant pressure traces from the other five locations; 200 traces were then ensembled from each location. The first cycles of all six 200-ensembled pressure traces are given in Fig. 12 with the horizontal axis plotted as position rather than time. This position was derived from the time history by multiplying the time by the convective velocity; in the present case, the convective velocity was 198.4 m/s (see Fig. 8).

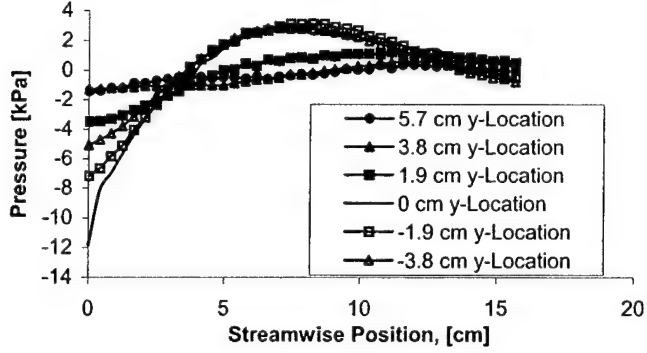


Figure 12. Average Coherent-Structure, Static-Pressure Well.

Unfortunately, our data acquisition card was only able to collect data after the trigger. As may be noted in Fig. 5, the static pressure well should not be symmetric in the up- and downstream directions; however, in order to get a sense of the pressure well shape for comparison with Fig. 5, we reflected the data from upstream into the downstream direction and plotted it as a surface similar to that in Fig. 5. The result is shown in Fig. 13, which shows a pseudo-reconstruction of a pressure well for an average coherent structure along with the computed well from Fig. 5; it is clear that the most controversial assertion of the model (i.e., that deep pressure wells are present in the shear layer) has been vindicated and that the depth of the pressure wells are in good agreement with the predictions of the Weakly-Compressible Model.

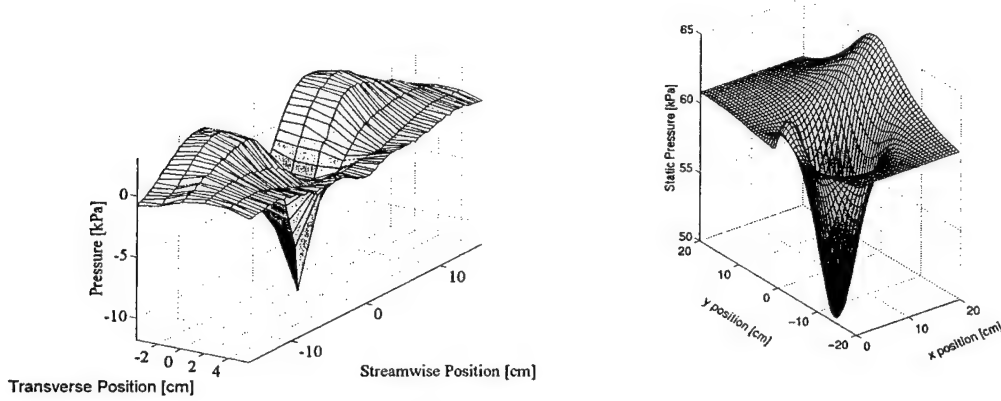


Figure 13. Pseudo-Reconstruction of the Static Pressure Well for an Average Coherent Structure (left) and the Static Pressure Well Predicted by the Weakly-Compressible Model (right).

**Aero-Optical Data.** In order to perform the aero-optical measurements, an optical bench was positioned under the test section and equipped with the various optical components needed to make the SABT measurement. Figure 14 shows a photograph of the SABT equipment in place below the shear layer test section. As described in detail in Reference 12, the SABT sensor makes use of a sparse array of sensors that measure the time history of the tilt of small aperture laser beams positioned along the streamwise direction, which are projected through the shear layer normal to the layer. The angle of tilt at a given location is the derivative of a wavefront of a large-aperture laser beam that could be made to propagate through the shear layer at that same instant. As described in Reference 12, in order to perform the integration of the wavefront's spatial derivative over the aperture of interest at any instant in time, position is exchanged for time by using the Taylor hypothesis. The use of the Taylor hypothesis is based on the fact, first noted by Malley [Ref. 11],

that aberrations on a wavefront associated with propagation through a convecting turbulent flow must themselves convect. In order to construct a wavefront over a 10 cm aperture, we determined that three small-aperture laser probe beams were required. With this in mind, Fig. 15 shows a schematic of the SABT optical bench. The schematic shows a single laser beam that is first run through a two-lens telescope and then is split into multiple beams before being directed off the optical bench and through the shear layer by a beam-steering mirror. After exiting the test section the beams are redirected onto the optical bench where they are individually directed onto lateral-effect detectors. The signals from the lateral-effect detectors, which contain position/tilt information, were then sent to transimpedance amplifiers where they were converted to voltage and read by the data acquisition system. In addition to the SABT beams, a separate laser beam was reflected off a mirror attached to the test section and directed onto a fourth lateral-effect detector; the signal from this detector was recorded and used to infer tunnel vibration.

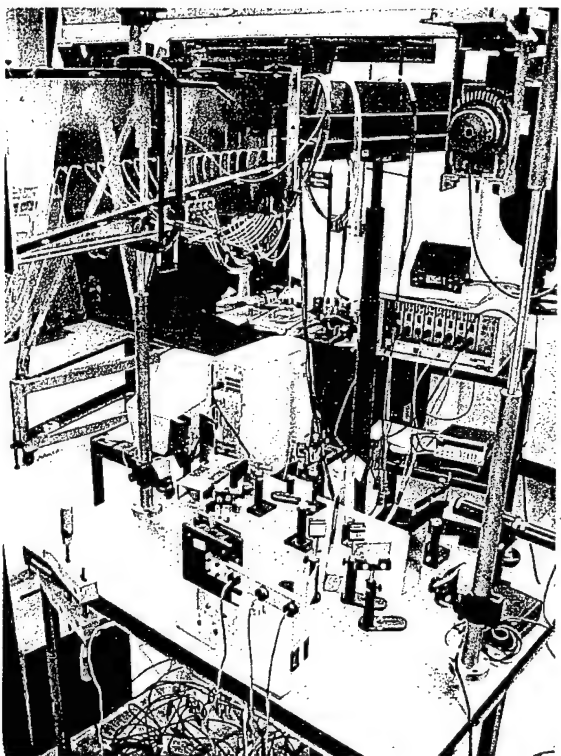


Figure 14. Transonic Shear Layer Facility with SABT equipment on optical bench.

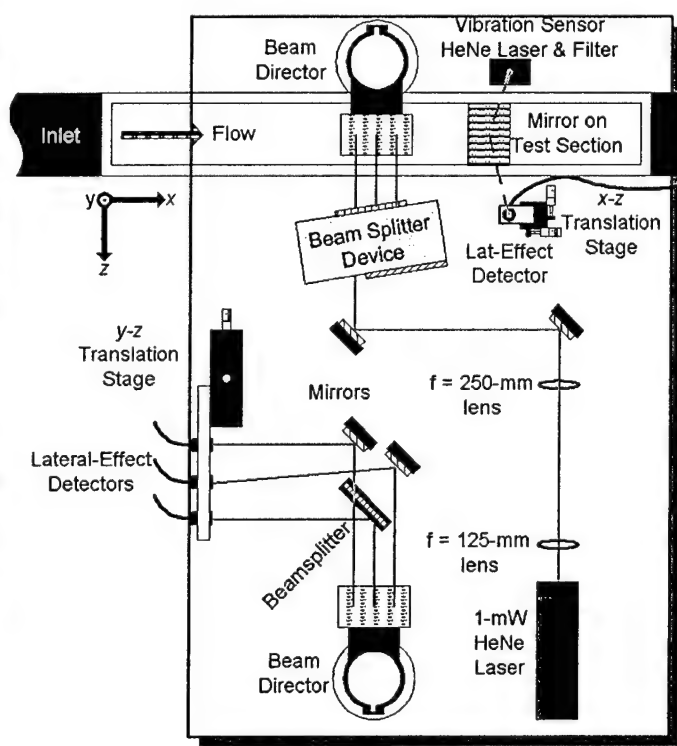


Figure 15. Plan-View Schematic of the SABT Optical Bench.

Wavefronts were constructed from the collected time series of wavefront derivatives using the procedure described in References 7, 17 and 24. The main uncertainty in the constructed wavefronts was the effect of the tunnel vibration. As described in References 17, 21 and 24, while more computationally-intensive coherency methods of vibration removal are possible, the intense vibration corruption associated with the AEDC data was able to be removed by applying a simple high pass filter. Our measurements of the vibration in the Notre Dame tunnel suggested that a filter at 750 Hz would again facilitate the removal of vibration corruption. As in the AEDC wavefront constructions, a series of wavefronts were constructed using progressively lower-frequency high pass filters. In the AEDC case, once this cutoff fell below the vibration frequency there was a very

distinct change in the level and character of the constructed wavefronts; in the present case, however, this sudden change of character did not appear.

Figures 16 – 19 give the result of filtering the slope data at successively lower cutoffs starting at 2 kHz and decreasing to zero. It should be noted that the aperture size for this series of figures was set at 5 cm in order to compare with the AEDC wavefronts given in Fig. 4. At the high end, Fig. 16 shows the effect of passing only those frequencies greater than 2 kHz. It should be noted that some structure is clearly present above this frequency. As discussed above, the primary fully-formed flow structures at the measurement location (centered at 0.5 m from the splitter plate) were at approximately 1.1 kHz; however, occasionally pairing events took place at this location, which could increase the frequency for the structures formed by the Kelvin-Helmholz instability above 2 kHz.

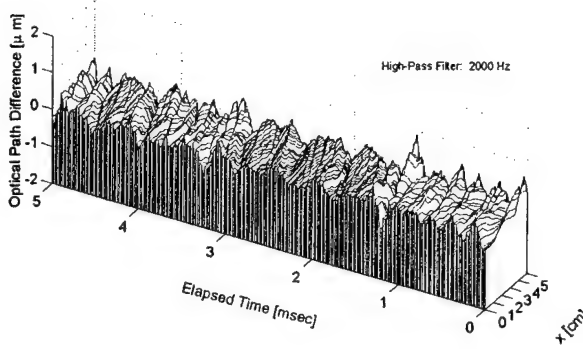


Figure 16. Notre Dame experimental wavefronts, high pass filter = 2000 Hz,  $\delta=2.5$  cm,  $U_c = 204.13$  m/s,  $M_c = 0.628$ ,  $OPD_{rms} = 0.169 \mu\text{m} \sim 0.267$  waves [Ref. 24].

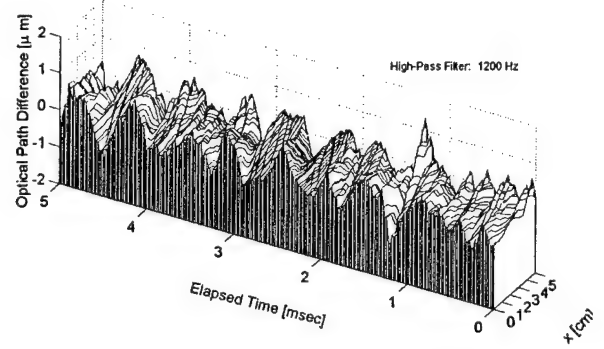


Figure 17. Notre Dame experimental wavefronts, high pass filter = 1200 Hz,  $\delta=2.5$  cm,  $U_c = 218.75$  m/s,  $M_c = 0.673$ ,  $OPD_{rms} = 0.258 \mu\text{m} \sim 0.408$  waves [Ref. 24].

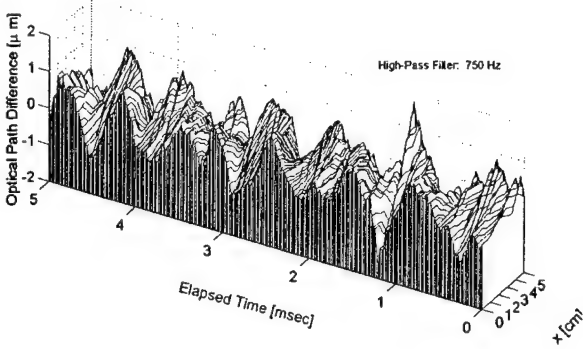


Figure 18. Notre Dame experimental wavefronts, high pass filter = 750 Hz,  $\delta=2.5$  cm,  $U_c = 218.17$  m/s,  $M_c = 0.671$ ,  $OPD_{rms} = 0.336 \mu\text{m} \sim 0.532$  waves [Ref. 24].

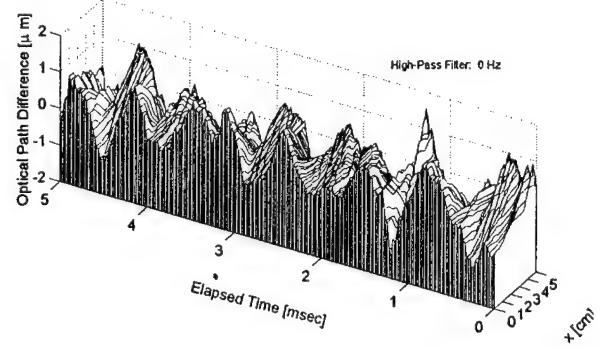


Figure 19. Notre Dame experimental wavefronts, high pass filter = 0 Hz (unfiltered),  $\delta=2.5$  cm,  $U_c = 216.40$  m/s,  $M_c = 0.666$ ,  $OPD_{rms} = 0.400 \mu\text{m} \sim 0.631$  waves [Ref. 24].

The structure in the wavefront time series of Fig. 16, at approximately 1.3 msec elapsed time, may be a pairing event; however, the predominant structures in the Fig. 16 time series with frequencies of above 4 kHz are probably due to turbulent-boundary-layer structures either fed into the shear layer at the splitter plate and/or the turbulent boundary layer on the high-speed tunnel wall, where the SABT beams emerge from the tunnel. If these are boundary-layer structures, it might be noticed that they are approximately 3 times as large as those from AEDC at the Station 1 location

(Fig. 2). As the cutoff frequency for the filter is reduced the wavefronts associated with the passage of the large-scale coherent structures can be seen to appear at 1.2 kHz (Fig. 17); however, the large tilt in the wavefront can be seen to be fully constructed by a cutoff of 750 Hz (Fig. 18). A reduction in the filter frequency to 0 Hz (Fig. 19) shows almost no change from that for the 750 Hz filter. Unlike the AEDC wavefront data, for whatever reason, no obvious effect of the vibration seemed to be present in these wavefronts.

**Aero-Optical Comparison with The Weakly-Compressible Model.** The conditions for these tests were simulated using the Weakly-Compressible Model, and the index-of-refraction field was integrated to produce time series of wavefronts. Figure 20 gives the first 3 msec of experimental wavefront data from Fig. 18, and Fig 21 shows predicted time series of wavefronts for the Notre Dame experimental-shear-layer conditions for the same time period, both presented to the same scale.

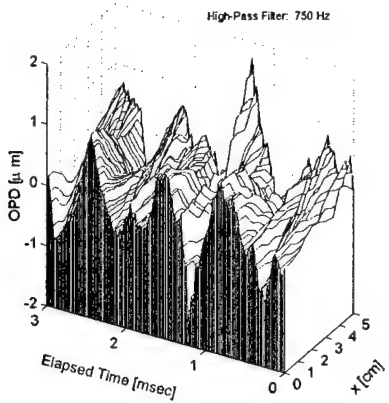


Figure 20. First 3 msec of Experimental Wavefronts from the Time Series in Figure 18.

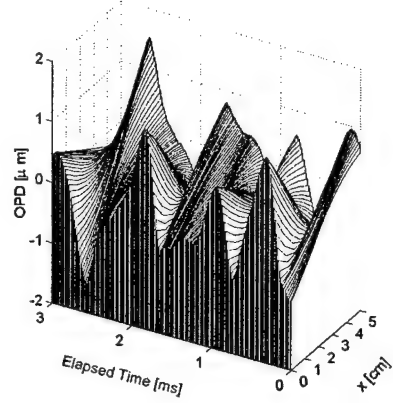


Figure 21 . Wavefronts Computed using the Weakly-Compressible Model Shear Layer for the Experimental Shear Layer Flow Conditions, for a 20 cm Aperture.

The similarity in the two time series of Figs. 20 and 21 is obvious. First, the peak-to-peak variation in OPD is uncannily similar in both time series. Also the predominant aberration is tilt and the apparent frequencies of the two series are similar. The main difference between the time series is the higher-frequency structure of the experimental wavefronts. These higher-frequency structures on the wavefronts are similar in character to those on the AEDC wavefronts referred to earlier; again, these are attributable to the turbulent boundary layers.

As large as the peak-to-peak OPD is in the wavefronts in Figs. 20 and 21, which show OPD's of as much as 3  $\mu$ m over the 5 cm aperture, it should be noted that they would be even larger for apertures large enough to capture a complete cycle of the disturbance. Figure 22 shows an extension of the wavefronts in Fig. 21 to a 20 cm aperture, where the peak-to-peak difference in the OPD over a 20 cm aperture can be seen to be as large as 5  $\mu$ m. These Notre Dame OPD's may be compared with the AEDC wavefronts, which were as large as 1.5  $\mu$ m over a 5 cm aperture and up to 3  $\mu$ m over a larger 20 cm aperture. This increase in the Notre Dame peak-to-peak OPD over those from the AEDC study is consistent with the predictions of the Weakly-Compressible Model. It should be further noted that this increase over the AEDC OPD's was actually somewhat mitigated by the fact that the Notre Dame conditions simulated flight at 22,300 ft altitude while the AEDC conditions were for a simulated altitude of 13,500 ft, since, as discussed in Reference 22, increasing altitude decreases OPD in direct proportion to the reduction in static density at altitude.

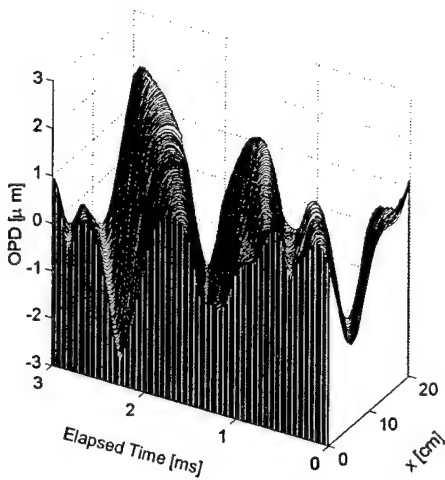


Figure 22. Wavefronts Computed using the Weakly- Compressible Model for the Experimental Shear Layer Flow Conditions, for a 20 cm Aperture.

**Validation of the Weakly-Compressible Model.** In addressing the first research objective of this grant period we were able to bring on line a new compressible shear layer facility and perform the first independent, time-resolved, aero-optical measurements for propagation through a compressible shear layer since the only other measurements of their kind were performed at AEDC in the mid 1990's. In addition, we made detailed fluid mechanic measurements to document the flow conditions, the formation of coherent shear-layer structures and the static pressure profiles through these structures. Taken together, the agreement with the Weakly-Compressible Model was extremely good. Not only did these series of tests validate the Weakly-Compressible Model, the static pressure data measured for the coherent structures were really the first experimental verification of the key assumption upon which the model was based: the presence of large static-pressure fluctuations within a high-Mach-number free shear layer, associated with the high curvature in the flow of the coherent, large-scale vortical structures. This demonstration that the static pressure fluctuations in free shear layers are anything but negligible, in and of itself is an important fluid-mechanic discovery and overturns decades of belief to the contrary embodied in the “*Strong Reynolds Analogy*.” Although predictable from the model, the now *measured* large peak-to-peak OPD's associated with this near-transonic shear layer sends an extremely strong message to those concerned with beam-control issues for laser systems intended for use on high-performance aircraft.

#### IV. OBJECTIVE 2: THE APPLICATION OF LOW-ORDER METHODS TO AERO-OPTICS

The second research objective for this reporting period was to investigate the use of low-order methods in describing the aero-optical environment associated with free shear layers. After studying a number of low-order approaches, because our studies had indicated that the most important aberration phenomena in shear layers are the coherent structures, which tend to be larger structures, Proper Orthogonal Decomposition (POD) seemed to show the most promise. The reason for this is that the use of POD in fluid mechanics showed that POD analysis was capable of capturing these larger-scale structures to great fidelity with only a few eigenmodes. It seemed clear to us that in order to apply

POD to the aero-optical problem we would need to have instant-to-instant information about the aberrating flowfield. We were faced with a decision to either use computed flow fields or experimental data; in fact, in the best situation would be the availability of both computational and experimental descriptions of an aberrating shear flow. Fortunately, we had available to us an excellent set of fluid-mechanic and optical data for the heated jet from an earlier grant period that seemed to lend itself to the POD study. From an application point of view, while the mechanism for causing the aberration in the heated jet is different than for the compressible shear layer, the spatial and temporal frequencies are scalable [Ref. 22]. Thus, we felt this earlier, heated-jet data was an excellent place to start an investigation whose outcome was anything but clear.

In particular, we had collected phase-locked temperature data for the jet under acoustic forcing. Using the acoustic forcing, we achieved regular, two-cycle periodic index-of-refraction fields, whose wavefronts were repeated over a 14-hour period while phase-locked temperature data were taken. Figure 23, is a time series of wavefronts from that forced study, along with selected realizations (from 256 such realizations) of the jet's temperature field, progressing in time from the top field to the bottom field [Ref. 25].

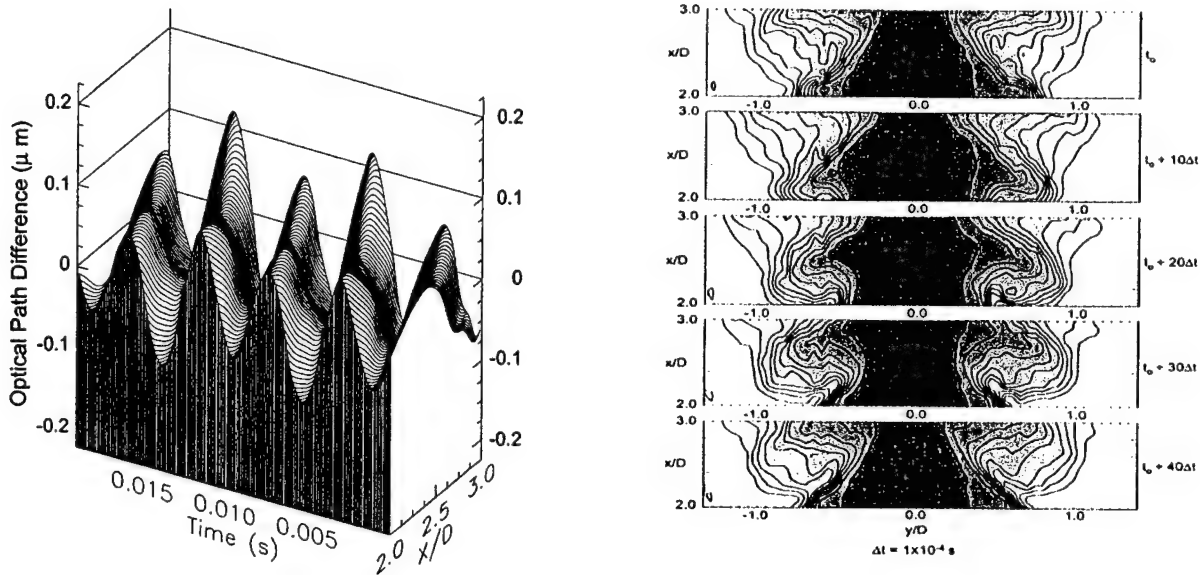


Figure 23. Time Series of Wavefronts for Propagation through Acoustically-Forced Heated Jet (left) and Selected Succession of Phase-Locked-Averaged Temperature Fields for the Same Jet (right) [Ref. 25]

The use of POD for various fluid mechanics problems is now relatively commonplace [Refs. 26-30]. It has been shown that complete descriptions of the various scalar and vector fields in a flow can be accurately reproduced using less than 14 eigenmodes, and occasionally less than eight. Generally, these eigenmodes operate in pairs. Once the number of modes required for a given accuracy are known, the various fields associated with the flow can be recreated by the superposition of these eigenmodes (multiplied by their appropriate temporal coefficients). Once eigenmodes are extracted from a flowfield, it is possible to extract the temporal coefficients by projecting experimental data onto the eigenmodes [Ref. 29,30]. In general, POD methods are computationally intensive, but have proven to be valuable in extracting the major structures present in a flow, and in this regard POD methods have proven to be valuable, albeit computationally intensive, to the study of fluid mechanics;

however, once the eigenmodes have been extracted, their use in acquiring the temporal coefficients from the flow, as in References 29 and 30, has been shown to be far less intensive.

If POD has proven to be valuable in fluid mechanics, our application of POD to the aero-optics problem must be described as magical. As described in detail in References 31 and 32, we first computed index-of-refraction fields from the temperature fields for the acoustically-forced heated jet. We then removed the average index-of-refraction over all realizations from each realization and applied POD analysis to the series of 256 average-removed, index-of-refraction fields (scalar fields) to determine the fields eigenmodes. Figure 24 shows an index field at one instant in time and the reconstructed field using a superposition of the first four, temporal-coefficient-weighted eigenmodes. It is clear that the first four modes capture much of the detail; however, approximately eight to twelve eigenmodes were needed to reduce the error to a point that the fields became “indistinguishable.”

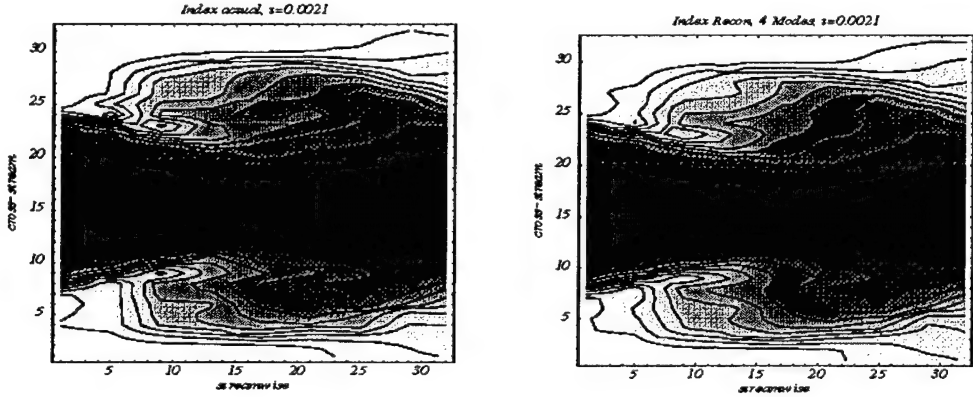


Figure 24. A Single Frame of Index of Refraction for the Flow field of Figure 23, Actual on Left (a) and 4-eigenmode Reconstruction on the Right (b) [Refs. 31,32].

On the other hand, the Optical Path Difference, OPD, associated with the two-dimensional index field is a one-dimensional field constructed by integrations through the index-of-refraction field in a particular direction. For example, the OPD( $x$ ) for projection normal to the flow, whose index field is represented by Fig. 24(a), would be represented by the dark line in Fig. 25(a). To the extent that detail along the path of integration through the index field is both above and below the mean index, integrations tend to remove the effect of detail along the path; this turns out to be the case for these index fields.

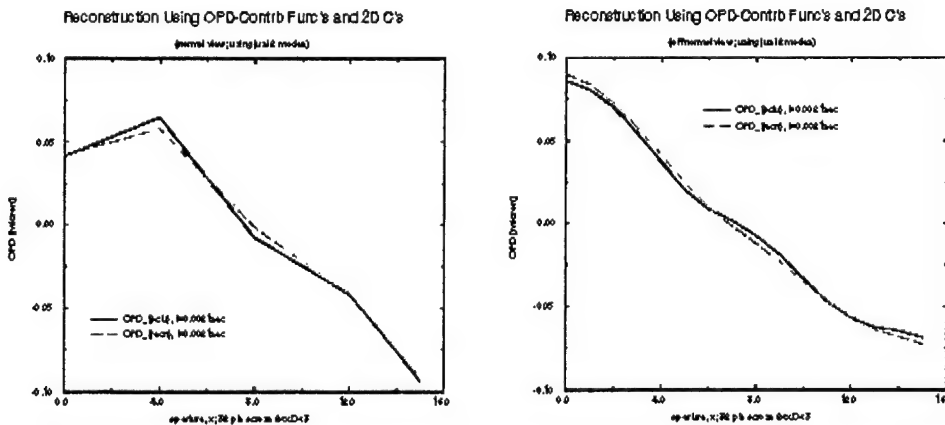


Figure 25. OPD's Constructed by Integration through the Full and 2-Eigenmode Index Fields for Normal Projection (left - a) and for Oblique Projection on the (right - b) [Ref. 31,32]

The lighter dashed curve in Fig. 25(a) is an OPD constructed using the index field reconstructed using *only the first two eigenmodes*. On average, the error in the 2-Mode OPD's was less than 1/100 micron; in general, wavefronts correct to better than 1/20 micron are considered sufficient for adaptive-optic corrections to laser systems whose wavelengths are near a micron. Figure 26 gives the first two eigenmodes for the index fields.

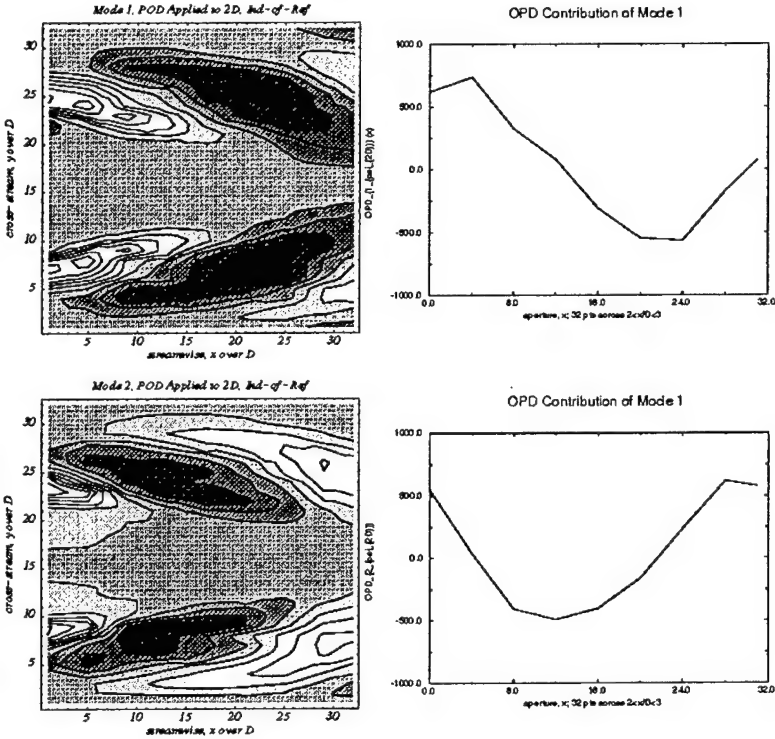


Figure 26. First Two Eigenmodes for the Index Field of the Figure 23 Flow and Corresponding OPD-Contribution Functions for Projection Normal to the Flowfield [Refs. 31,32]

We then discovered that the OPD's can be constructed by first integrating through the individual eigenmodes to produce OPD-contribution functions, and using the index-field's, self-same temporal coefficients to construct the OPD. Again, only the first two OPD-contribution functions were needed to obtain the accuracy as before. It then dawned on us that OPD-contribution functions in any oblique angle were possible by integrating through the eigenmodes in any oblique direction of interest to obtain oblique OPD-contribution functions in that direction. The oblique OPD constructions using only the first two eigenmodes turned out to be as accurate as the normal OPD constructions using only the first two eigenmodes. Although in retrospect, this result might seem to be intuitive because of the linearity of the optical problem, this result represents a major discovery.

Figure 27 shows the first OPD-contribution function for a normal projection and an oblique projection through the first eigenmode. The conclusion is inescapable, *if sufficient knowledge of the flowfield is available to extract the first few eigenmodes of the flow, then, if the temporal coefficients can be extracted through the use of a beacon, for example, in a fixed direction, these can be used to infer the wavefront in any other oblique direction*.

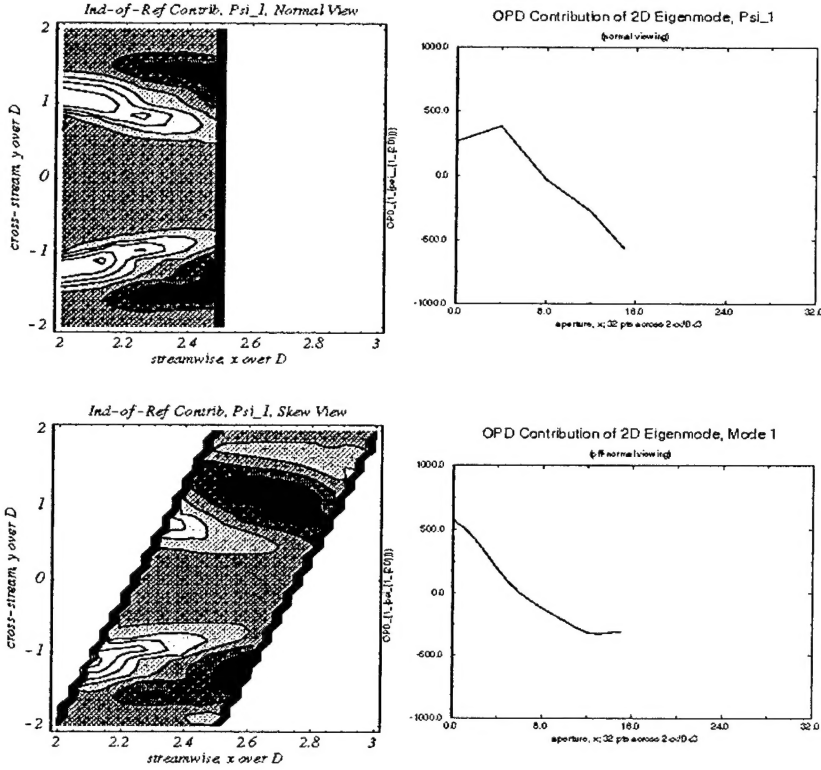


Figure 27. First OPD-Contribution Function for the First POD Eigenmode of the Index Field for Normal Projection (top - a) and for an Oblique Projection (bottom - b) [Refs. 31,32]

Near the end of the POD study, we took a cursory look at a method of inferring the OPD using a very-sparse sensor. We chose a limited number of locations along the aperture and constructed wavefront-slope contribution functions from the first two OPD-contribution functions. Knowing that a) the wavefront and its concomitant slopes were accurately described by the use of only the first two OPD-contribution functions, and b) the actual wavefront slopes at these limited number of measurement locations had to be made up of a linear combination of two slope contribution functions, it was possible to estimate the temporal coefficients to relatively high accuracy by using an optimized fit to the limited locations [Ref. 33].

## V. CONCLUDING REMARKS

The research in this reporting period has yielded a number of important breakthroughs in the field of aero-optics. The Weakly-Compressible Model has clearly been validated and in the process a longstanding misconception about the nature of static pressure fluctuations in a free shear layer has been set straight. This validation also produced the first independent wavefront data for a high, subsonic Mach number free shear layer since the data also collected by Notre Dame at the AEDC compressible shear layer facility. These new data reinforced the alarming message that aero-optical aberrations associated with lasers on high-performance aircraft pose a major design consideration. In addition to this validation, this reporting period has also produced the first application of POD methods to the aero-optics problem. This first study has proven to have important implications to practical solutions to determining the wavefront aberrations due only to the aero-optic flow field in the vicinity of the aircraft by the possible use of a beacon. Although not specifically noted, these early

POD results have clear application to the possible use of adaptive optics to mitigate the aero-optic affects.

Finally, it should be noted that Notre Dame will soon be taking possession of a high-bandwidth adaptive-optic system being built by Xinetics and Boeing under a DURIP grant obtained in conjunction with the grant reported on in this report (DURIP Grant Number F49620-01-0323). The new adaptive-optic (A-O) system will be used in the follow-on effort to the effort reported on here. Figure 28 shows a schematic of how we plan to use the new A-O system, in conjunction with acoustic forcing, on the heated jet to experimentally study some techniques suggested by the POD results referred to above, particularly with regard to oblique propagation.

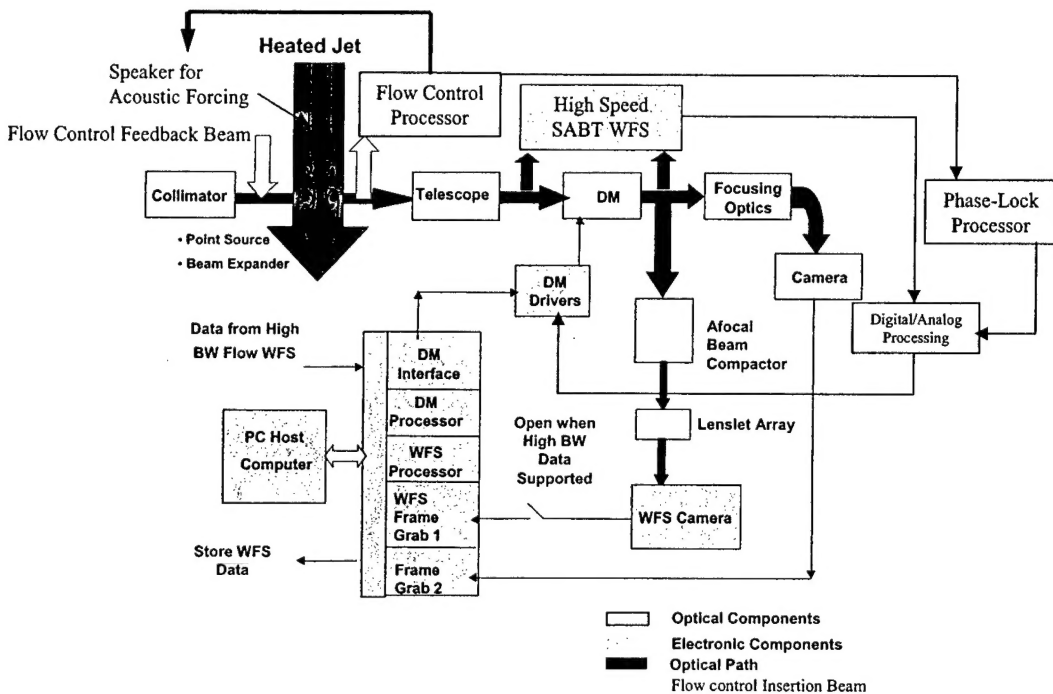


Figure 13. Proposed Experimental Set Up to Demonstrate Adaptive-Optical Wavefront Compensation for Laser Propagation Through a Heated Jet.

**Personnel Supported under this Effort.** In addition to providing approximately one month of summer support each year to the Principal Investigator, Eric J. Jumper, the grant supported a Masters student for approximately one year, M. Chouinard, a PhD student for approximately one and a half years, J. Cicchiello, and a second PhD student for a little over one year, J. Siegenthaler.

**Dissemination of Results.** This research produced a PhD Dissertation [Ref. 33] and ten technical papers [Refs. 18,19,20,21,22,23,24,25,31,32], six of which are in journals. Several more papers are in various stages of review by journals. Notre Dame has also kept close ties with Dr. L.D. Weaver of the AF Research Laboratory, Kirtland AFB, NM.

## REFERENCES

1. Smith, W.J., *Modern Optical Engineering: the Design of Optical Systems*, McGraw-Hill, New York, 1966.
2. Sutton, G.W., "Effects of turbulent fluctuations in an optically active fluid medium," *AIAA Journal*, 7(9), pp. 1737-1743, 1969.
3. Tatarski, V.I., *Wave Propagation in Turbulent Medium*, Dover, New York, 1961.
4. Tyson, R.K., *Principles of Adaptive Optics*, Academic Press, Inc., San Diego, 1991.
5. Tyson, R.K., "The status of astronomical adaptive optics systems," *O.E. Reports*, 121, pp. 11,13, Jan 1994.
6. Verhoff, A., "Prediction of optical propagation losses through turbulent boundary/shear layers," in *Aero-Optical Phenomena*, Gilbert and Otten, eds, Progress in Astronautics and Aeronautics Series 80, pp. 40-77, AIAA, Inc., New York, 1982.
7. Hugo, R.J., and Jumper, E.J., "Experimental measurement of a time-varying optical path difference by the small-aperture beam technique," *Applied Optics*, 35, pp. 4436-4447, August 1996.
8. Liepmann, H.W., "Deflection and diffusion of a light ray passing through a boundary layer," Report SM-14397, Douglas Aircraft Company, Santa Monica Division, Santa Monica, California, May 1952.
9. Havener, G., "Optical wave front variance: a study on analytic model in use today," *AIAA Paper 92-0654*, Jan 1992.
10. Klein, H.H., Malley, M.M., Sapp, O., Shough, D., Sutton, G.W. and Yu, J. H.-Y., "Experimental measurements of the optical path difference of a four-meter dual aerocurtain," *Proceedings of the High Power Laser Optical Components conference*, boulder, Colorado, Oct 1989.
11. Malley, M. Sutton, G.W. and Kincheloe, N., "Beam-Jitter measurements of turbulent aero-optical path differences," *Applied Optics* 31, pp. 4440-4443, 1992.
12. Jumper, E.J., and Hugo, R.J., "Quantification of aero-optical phase distortion using the small-aperture beam technique," *AIAA Journal*, 33(11), pp. 2151-2157, 1995.
13. Fitzgerald, E.J., and Jumper, E.J., "Two-dimensional, Optical Wavefront Measurements Using a Small-Aperture Beam-Technique-Derivative Instrument," *Optical Engineering*, 39 (12), December 2000, pp.3285-3293.
14. Cicchiello, J.M., and Jumper, E.J., "Far-Field Optical Degradation due to Near-Field Transmission Through a Turbulent Heated Jet," *Applied Optics*, 36 (25), pp. 6441-6452, September 1997.
15. Goodman, J.W., *Introduction to Fourier Optics*, McGraw-Hill, NY, 1968.
16. Yanta, W.J., Spring, W.C., Lafferty, J.F., Collier, A.S., Bell, R.L., Neal, D.R., Hamrick, D.R., Copland, R.J., Pezzaniti, L., Banish, M. and Shaw, R., "Near- and Farfield Measurements of Aero-Optical Effects Due to Propagation Through Hypersonic Flows," *AIAA Paper 2000-2357*.
17. Jumper, E.J., Hugo, R.J., Havener, G. and Stepanek, S.A., "Time-Resolved Wavefront Measurements through a Compressible Free Shear Layer," *AIAA Journal* , 35 (4), April 1997, pp. 671-677.

18. Cicchiello, J.M., Fitzgerald, E.J. and Jumper, E.J., "Far-Field Implications of Laser Transmission Through a Compressible Shear Layer," *Free-Space Laser Communication Technologies XIII Conference*, **4272**, SPIE, San Jose California, 20-26 January 2001, pp. 245-259.
19. Fitzgerald, E. J. and Jumper, E. J., "Further Consideration of Compressibility Effects on Shear-Layer Optical Distortion," AIAA Paper 99-3617, June 1999.
20. Jumper, E.J., and Fitzgerald, E.J., "Recent Advances in Aero-Optics," *Progress in Aerospace Sciences*, **37**, 2001, pp. 299-339.
21. Fitzgerald, E.J. and Jumper, E.J., "Aperture Effects on the Aerooptical Distortions Produced by a Compressible Shear Layer, *AIAA Journal*, **40** (2), Feb 2002, pp. 267-265.
22. Fitzgerald, E.J. and Jumper, E.J., "Scaling Aerooptic Aberrations Produced by High-Subsonic-Mach Shear Layers," *AIAA Journal*, **40** (7), July 2002, pp. 1373-1381.
23. Chouinard, M. Asghar, A., Kirk, J.F., Siegenthaler, J.P. and Jumper, E.J., "An Experimental Verification of the Weakly-Compressible Model, AIAA Paper 2002-0352, Jan 2002.
24. Fitzgerald, E.J., Siegenthaler, J.P. and Jumper, E.J., "Optical Characterization of the Notre Dame Compressible Shear-Layer Facility," AIAA Paper 2002-2274, May 2002.
25. Hugo, R.J. and Jumper, E.J., "Applicability of the Aero-Optic Linking Equation to a Highly Coherent, Transitional Shear Layer," *Applied Optics*, **39** (24), August 2000, pp. 4392-4401.
26. Lumley, J., "The Structure of Inhomogeneous Turbulent Flows," *Proceedings of the International Colloquium of the Fine Scale Structure of the Atmosphere and its Influence on Radio Wave Propagation*, ed. A.M. Yaglam, V.I. Tatarsky, Dklay Akademii Nauk SSSR, Moscow, Nauka, pp. 166-178, 1967.
27. Berkooz, G., Holmes, P., Lumley, J., "The Proper Orthogonal Decomposition in the Analysis of Turbulent Flows," *Ann. Rev Fluid Mech*, **25**, pp. 539-575, 1993.
28. Gordeyev, S.V. and Thomas, F.O., "Coherent Structure in the Turbulent Planar Jet, Part 1. Extraction of Proper Orthogonal Decomposition Eigenmodes and Their Self-Similarity," *J Fluid Mech*, **414**, pp. 145-194, 2000.
29. Gordeyev, S.V. and Thomas, F.O., "Coherent Structure in the Turbulent Planar Jet, Part 2 Structural Topology via POD Eigenmode Projection," *J Fluid Mech*, 2002.
30. Arndt, R.E.A., Long, D.F., Glauser, M.N., "The Proper Orthogonal Decomposition of Pressure Fluctuations Surrounding a Turbulent Jet," *J. Fluid Mech.*, **340**, pp. 1-33, 1997.
31. Cicchiello, J.M. and Jumper, E.J., "Low-Order Representation of Fluid-Optic Interactions Associated with a Shear Layer," AIAA Paper 2001-0952, Jan 2001.
32. Cicchiello, J.M. and Jumper, E.J., "Addressing the Oblique-Viewing Aero-Optic Problem with Reduced-Order Methods," AIAA Paper 2001-2799, June 2001.
33. Cicchiello, J.M., *Low-Order Representation of Dynamic Aero-Optic Distortions*, PhD Dissertation, University of Notre Dame, April 2001.